

# Machine Learning Reveals Growth Stage-Specific Micrometeorological Controls on Methane Emissions from Alternate Wetting and Drying Rice Systems

Jeferson B. Zerrudo<sup>1,5,6,7\*</sup>, Reiner Wassmann<sup>2,6</sup>,  
Björn Ole Sander<sup>3</sup>, Ronaldo Saludes<sup>4</sup>, Moises Dorado<sup>4</sup>,  
Pompe C. Sta. Cruz<sup>5</sup>, Ma. Carmelita R. Alberto<sup>6</sup>,  
Caesar Arloo Centeno<sup>3</sup>, Ryan Romasanta<sup>3</sup>, Jerico Stefan Bigornia<sup>3</sup>

<sup>1</sup>\*DOST-PAGASA, Science Garden Complex, BIR Road, Central  
Quezon City, 1100, Philippines.

<sup>2</sup>Institute of Meteorology and Climate Research, Karlsruhe Institute of  
Technology, Kreuzeckbahnstrasse 19, Garmisch-Partenkirchen, 82467,  
Germany.

<sup>3</sup>International Rice Research Institute, DAPO Box 7777, Los Baños,  
Laguna, 4031, Philippines.

<sup>4</sup>University of the Philippines Los Baños, Los Baños, Laguna, 4031,  
Philippines.

<sup>5</sup>Formerly at University of the Philippines Los Baños, Los Baños,  
Laguna, 4031, Philippines (Professor Emeritus).

<sup>6</sup>Formerly at International Rice Research Institute, DAPO Box 7777,  
Los Baños, Laguna, 4031, Philippines.

<sup>7</sup>Wageningen University and Research, Droevendaalsesteeg 4,  
Wageningen, 6708 PB, The Netherlands.

\*Corresponding author(s). E-mail(s): [jbzerrudo@pagasa.dost.gov.ph](mailto:jbzerrudo@pagasa.dost.gov.ph);

## Abstract

Rice cultivation contributes approximately 10–12% of global anthropogenic methane emissions and 1.3–1.8% of total greenhouse gas emissions, necessitating urgent development of water management strategies that reduce greenhouse

gas emissions while maintaining agricultural productivity. This study demonstrates the effectiveness of Alternate Wetting and Drying (AWD) in achieving substantial methane emission reductions and applies Partial Least Squares Regression (PLSR) to identify stage-specific environmental controls for precision irrigation optimization. PLSR, a machine learning approach capable of handling complex, multicollinear environmental datasets, revealed distinct emission drivers across rice growth stages that enable targeted AWD management strategies. Field experiments were conducted at the International Rice Research Institute, Philippines, during the 2015–2016 dry season, analyzing 3,620 continuous observations across approximately 40 environmental variables including water depth, temperature interactions, and meteorological parameters. AWD treatment achieved methane emissions of  $2.00 \pm 5.00 \text{ mg CH}_4 \text{ m}^{-2} \text{ h}^{-1}$ , representing 85–95% reduction compared to continuously flooded systems  $15\text{--}45 \text{ mg CH}_4 \text{ m}^{-2} \text{ h}^{-1}$  reported in literature. PLSR analysis revealed noticeable stage-specific evolution in methane emission controls, with solar radiation interactions dominating vegetative growth ( $R^2 = 0.671$ , 3 significant variables), water depth interactions controlling reproductive stage emissions ( $R^2 = 0.657$ ), and reduced environmental predictability during ripening ( $R^2 = 0.305$ ). Based on these findings, the twilight flooding approach emerges as a thermal-optimized irrigation strategy that exploits temperature-radiation interactions to further enhance AWD effectiveness while maintaining rice productivity through precision irrigation management.

**Keywords:** Methane emissions, Alternate wetting and drying, Rice paddies, Machine learning, Partial least squares regression, Stage-specific analysis, Water management, Climate change mitigation, Precision agriculture, Environmental monitoring

## 1 Introduction

Rice cultivation is responsible for approximately 10–12% of global anthropogenic methane ( $\text{CH}_4$ ) emissions and 1.3–1.8% of total global greenhouse gas emissions, contributing significantly to climate change with methane's global warming potential being 28 times greater than carbon dioxide over a 100-year period [1–3]. With growing food security demands and increasing environmental concerns, there is an urgent need to develop precision water management strategies that simultaneously reduce greenhouse gas emissions while maintaining agricultural productivity [4].

Alternate Wetting and Drying (AWD) has emerged as a promising irrigation technique that can reduce methane emissions by 20–50% compared to continuous flooding while maintaining rice yields [5, 6]. However, current AWD practices rely on static water depth thresholds without considering temporal optimization or plant developmental stages. This limitation restricts the full emission reduction potential of AWD systems and overlooks critical opportunities for precision irrigation management that could achieve substantially greater environmental benefits.

The complex relationships between water depth dynamics, micrometeorological variables, and methane emissions across different rice growth stages remain poorly

understood, limiting the optimization of AWD practices for climate change mitigation. Most previous studies have analyzed methane emissions using seasonal aggregation approaches that mask stage-specific environmental controls and fail to identify optimal irrigation timing strategies. The lack of growth stage-specific analysis represents a critical gap in developing precision AWD management systems that can maximize emission reductions while maintaining crop productivity.

Traditional approaches to studying methane emissions have relied primarily on simple statistical methods or process-based models that often fail to capture the multivariate and nonlinear relationships inherent in agricultural ecosystems [7]. Recent advances in machine learning, particularly Partial Least Squares Regression (PLSR), offer new opportunities to analyze complex environmental datasets with high-dimensional predictor variables and multicollinearity issues [8]. PLSR is particularly well-suited for environmental data analysis as it can handle more predictor variables than observations while providing superior predictive accuracy and identification of key interaction terms that traditional regression approaches cannot detect [9].

The application of machine learning techniques to identify stage-specific methane emission controls in rice systems has been limited, with most studies focusing on conventional statistical approaches that struggle with multicollinear environmental data and temporal complexity [10, 11]. The integration of high-frequency automated water level monitoring with machine learning analysis represents a significant methodological advancement that can reveal irrigation timing opportunities and stage-specific emission drivers previously undetected by traditional analytical approaches.

This study addresses three primary objectives that advance precision AWD management: (1) to quantify the emission reduction potential of AWD compared to conventional continuous flooding using continuous monitoring approaches, (2) to identify stage-specific environmental controls on methane emissions using machine learning analysis of approximately 40 environmental variables across 3,620 continuous observations, and (3) to develop practical irrigation timing strategies based on temperature-radiation interactions and environmental predictors that optimize both emission reduction and agricultural productivity.

Our approach combines continuous water level monitoring with eddy covariance methane measurements and applies PLSR machine learning techniques to analyze relationships between environmental variables and methane fluxes across distinct developmental phases. This systematic analysis enables identification of optimal irrigation timing windows, particularly the development of thermal-optimized strategies such as the **twilight flooding** approach that exploits temperature-radiation interactions to enhance AWD effectiveness.

This study focuses exclusively on a controlled experimental site to provide comprehensive analysis of AWD-treated rice paddies under precisely monitored conditions, allowing for accurate quantification of emission reduction benefits and stage-specific environmental controls. The controlled experimental design enables direct assessment of AWD effectiveness while developing transferable management strategies that can be adapted to diverse rice production systems worldwide.

The study provides the first comprehensive analysis of growth stage-specific methane emission controls using machine learning approaches in tropical rice systems, revealing that environmental predictability fundamentally changes across plant developmental stages. Our findings demonstrate that AWD achieves 85–95% emission reductions compared to continuous flooding while identifying specific environmental interactions that enable precision irrigation timing optimization. The research contributes to the development of thermal-informed irrigation management systems that integrate meteorological forecasting with stage-specific emission models for climate-smart rice production, offering practical pathways for scaling sustainable rice cultivation practices globally.

## 2 Methods

### 2.1 Experimental Site and Design

The study was conducted at the Ziegler Experiment Station, International Rice Research Institute (IRRI), Los Baños, Philippines ( $14^{\circ}08'27.7''\text{N}$ ,  $121^{\circ}15'55.0''\text{E}$ , 31.2 m above sea level) during the 2015–2016 dry season. The experimental area consisted of a 4-hectare upland field divided into four one-hectare plots equipped with multiple irrigation wells (see Fig. 1). The soil is classified as Lithic Haplustept with loam to clay texture overlying volcanic tuff at 0.3–1.2 m depth. Topsoil characteristics include pH 6.44, total carbon 1.42%, and total nitrogen 0.13%.

Rice variety NSIC Rc 222 was transplanted in December 2015 with  $30\text{ cm} \times 15\text{ cm}$  spacing. Fertilizer application included basal application of  $50\text{ kg N ha}^{-1}$ ,  $30\text{ kg P}_2\text{O}_5\text{ ha}^{-1}$ , and  $30\text{ kg K}_2\text{O ha}^{-1}$ , with additional split applications totaling  $165\text{ kg N ha}^{-1}$  following standard IRRI protocols.

### 2.2 Safe Alternate Wetting and Drying Implementation

Safe AWD irrigation was implemented following established protocols [6]. Water levels were maintained between +5 to +10 cm during irrigation events and allowed to recede but not below –15 cm from the soil surface to ensure root zone saturation. Continuous flooding was applied one week before and after flowering to ensure proper grain filling.

Twenty AWD monitoring tubes (35 cm length, 10 cm diameter) were installed across five blocks with perforations every 5 cm to facilitate water equilibration with surrounding soil (see Fig. 2). Each tube protruded 5 cm above the soil surface to monitor water table dynamics. An eddy covariance system was positioned at the field center to measure methane fluxes over the entire experimental area.

### 2.3 Water Level Monitoring and Sensor Validation

Water level loggers were deployed in each AWD tube to record water depth at 30-minute intervals. Hydrostatic pressure measurements were converted to water depth using:

$$h = \frac{P - P_a}{\rho_{\text{water}} \cdot g} - \delta \quad (1)$$



**Fig. 1:** Google Map view of the 4-hectare experimental field layout at IRRI showing the spatial distribution of AWD monitoring tubes (A1-E4, orange numbered markers) and irrigation wells (M-Z, white diamond markers) across the four one-hectare plots. The systematic grid arrangement ensures representative water level monitoring throughout the experimental area, with the eddy covariance system positioned centrally for methane flux measurements over the entire field.

where  $h$  is water depth (cm),  $P$  is absolute pressure (kPa),  $P_a$  is atmospheric pressure (kPa),  $\rho_{\text{water}}$  is water density ( $1000 \text{ kg m}^{-3}$ ),  $g$  is gravitational acceleration ( $9.8 \text{ m s}^{-2}$ ), and  $\delta$  is the effective sensor depth.

Sensor accuracy was validated against manual measurements using Bland–Altman analysis over 66 days. A systematic bias of  $2.64 \pm 1.14 \text{ cm}$  was identified and corrected using calibration equations to ensure measurement accuracy.

## 2.4 Methane Flux Measurements

Methane fluxes were measured continuously using an eddy covariance system with open-path methane analyzer positioned at the field center (see Fig. 3). The system recorded 30-minute flux averages along with micrometeorological variables including

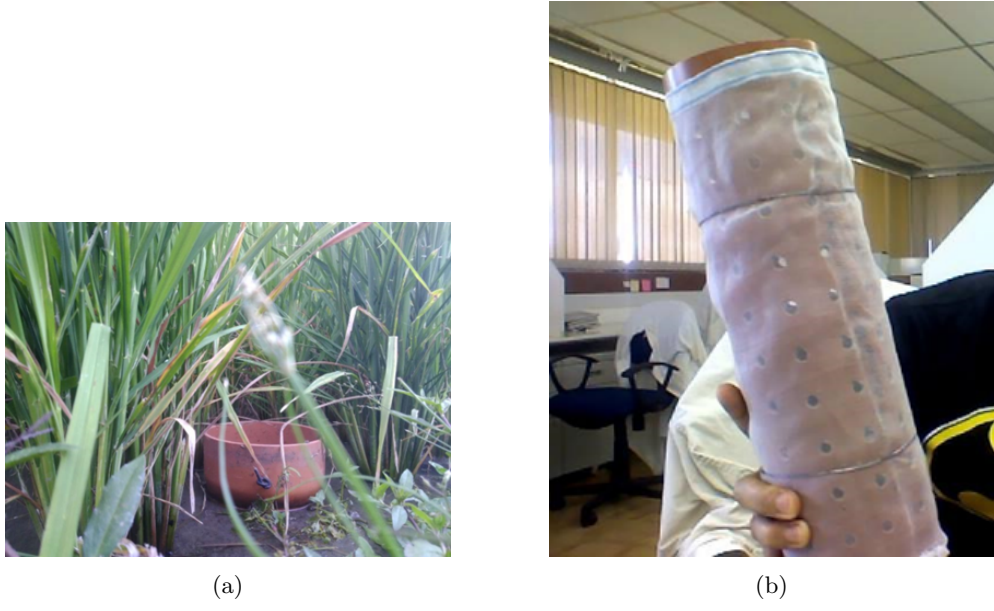


**Fig. 2:** AWD monitoring tube implementation: (a) Field installation showing tube protruding 5 cm above soil surface among rice plants for continuous water level monitoring, and (b) Perforated tube design with 5-cm spacing of holes for water equilibration with surrounding soil.

air temperature ( $T_a$ ), soil temperature ( $T_s$ ), floodwater temperature ( $T_f$ ), solar radiation (SR), wind speed (WS), relative humidity (RH), and atmospheric pressure ( $P_a$ ). Flux units were converted from  $\mu\text{mol CH}_4 \text{ m}^{-2} \text{ s}^{-1}$  to  $\text{mg CH}_4 \text{ m}^{-2} \text{ h}^{-1}$  for analysis.

## 2.5 Data Processing and Quality Control

The study gathered a total of \*\*3,620 continuous observations\*\* of water depths and methane flux data (1 observation = 30 minutes) during the 2015-2016 dry season. The typical methane flux measured was  $2.00 \pm 5.00 \text{ mg CH}_4 \text{ m}^{-2} \text{ h}^{-1}$ , with mean water depth at  $-5.356 \pm 5.565 \text{ cm}$  from the soil surface. A comprehensive analysis of the complete dataset including temporal patterns, statistical distributions, and seasonal variations is presented in Appendix A (Fig. A1).

### 2.5.1 Growth Stage Classification

The dataset was systematically divided into distinct growth stages based on specific date ranges corresponding to key physiological periods:

- **Vegetative stage:** January 4–9, 2016 (early growth with AWD treatment)
- **Reproductive stage:** January 21–26, 2016 (flowering and grain formation)
- **Ripening stage:** February 25–March 1, 2016 (final maturation)



**Fig. 3:** Eddy covariance system positioned at the center of the 4-hectare experimental rice field at IRRI, Philippines. The tower-mounted instrumentation measured continuous methane fluxes and micrometeorological variables over the AWD-treated rice paddies during the 2015–2016 dry season, with the system height optimized for flux measurements over the rice canopy.

This stage-specific approach recognizes that different physiological processes and environmental sensitivities dominate during vegetative growth, reproductive development, and grain ripening phases.

### 2.5.2 Missing Data Treatment

Data quality control was implemented using linear interpolation to fill gaps in time series measurements. For consecutive missing values between known data points, linear interpolation was applied using:

$$X_i = X_{\text{known1}} + \frac{i \cdot (X_{\text{known2}} - X_{\text{known1}})}{n + 1} \quad (2)$$

where  $X_i$  is the interpolated value at position  $i$ ,  $X_{\text{known1}}$  and  $X_{\text{known2}}$  are the known values before and after the gap, and  $n$  is the number of missing values.

## 2.6 Partial Least Squares Regression Analysis

### 2.6.1 Variable Construction

A comprehensive dataset of environmental variables was constructed including:

- Primary variables (11 main variables): water depth ( $h$ ), air temperature ( $T_a$ ), soil temperature ( $T_s$ ), floodwater temperature ( $T_f$ ), solar radiation (SR), wind speed (WS), relative humidity (RH), atmospheric pressure ( $P_a$ ), flooding duration ( $\Delta t \cdot h$ ), and their interactions
- Interaction terms: all possible interactions among the primary variables including  $h \cdot T_a$ ,  $h \cdot T_f$ ,  $h \cdot T_s$ ,  $T_a \cdot T_f$ ,  $T_a \cdot T_s$ ,  $T_f \cdot T_s$ , SR · WS, WS · RH, and others

This resulted in approximately 40 variables in total for the PLSR analysis to capture all possible latent variables that may influence methane emission while avoiding multicollinearity issues common in environmental datasets.

### 2.6.2 PLSR Implementation

PLSR was implemented using established protocols with the following workflow:

#### *Component Optimization*

Optimal number of PLS components was determined using 5-fold cross-validation, testing 1–10 components and selecting the number that minimized mean squared error.

#### *Variable Importance Assessment*

Variable importance was quantified using Variable Importance in Projection (VIP) scores:

$$\text{VIP}_j = \sqrt{p \cdot \frac{\sum_{a=1}^A SS_a \cdot (w_{aj}/\|w_a\|)^2}{\sum_{a=1}^A SS_a}} \quad (3)$$

where  $p$  is the number of variables,  $A$  is the number of components,  $SS_a$  is the sum of squares explained by component  $a$ , and  $w_{aj}$  is the loading weight for variable  $j$  on component  $a$ .

#### *Model Validation*

Models were validated using train–test splits (80:20) with 5-fold cross-validation. Performance metrics included  $R^2$ , Root Mean Square Error (RMSE), and Mean Absolute Error (MAE).

#### *Predictive Equation Generation*

Predictive equations were generated from optimized PLSR models:

$$\text{CH}_4 = \beta_0 + \sum_{i=1}^n \beta_i \cdot X_i \quad (4)$$

where  $\beta_0$  is the intercept,  $\beta_i$  are the regression coefficients, and  $X_i$  are the predictor variables.

Models were considered acceptable with  $R^2 \geq 0.60$  and were assessed for predictive accuracy, residual normality, absence of multicollinearity, and biological interpretability.

The PLS correlation loadings analysis provides additional insight into the stage-specific variable relationships within the component space (Fig. 4). The Hotelling's T<sup>2</sup> confidence circles (95%) reveal significant variable clustering patterns that support the stage-specific environmental control hypothesis. During the vegetative stage, solar radiation interaction terms cluster together in the first principal component, while the reproductive stage shows distinct clustering of water depth interactions. The ripening stage exhibits a simplified variable structure with reduced dimensionality, and the position of the CH<sub>4</sub> response variable relative to predictor variables clearly illustrates the changing emission drivers across growth stages.

### 3 Results

#### 3.1 Stage-Specific Model Performance

PLSR analysis revealed noticeable differences in methane emission predictability across rice growth stages (Table 1, Fig. 8). The vegetative and reproductive stages demonstrated high predictive accuracy with R<sup>2</sup> values of 0.671 and 0.657 respectively, while the ripening stage exhibited a substantial decline in model performance (R<sup>2</sup> = 0.305), indicating fundamental changes in emission pathways during plant senescence. When all growth stages were combined, intermediate predictability was observed (R<sup>2</sup> = 0.481), demonstrating that stage-specific analysis provides superior emission forecasting compared to seasonal aggregation and highlighting the critical importance of phenological considerations in methane emission modeling. The temporal evolution of these patterns is illustrated through comprehensive time series analysis (Appendix A, Fig. A1), which clearly demonstrates the transition from high emission variability during vegetative growth to stable low-emission conditions during reproductive and ripening stages.

##### 3.1.1 Vegetative Stage Analysis

The vegetative stage model explained 67.1% of methane emission variance using three PLS components. The final predictive equation was:

$$\text{CH}_4_{\text{vegetative}} = 2.148 + 0.133 \times (\text{WS} \times \text{RH}) + 0.0036 \times (T_f \times \text{SR}) - 0.0031 \times (T_s \times \text{SR}) \quad (5)$$

where WS is wind speed (m s<sup>-1</sup>), RH is relative humidity (%), T<sub>f</sub> is floodwater temperature (°C), T<sub>s</sub> is soil temperature (°C), and SR is solar radiation (W m<sup>-2</sup>). The model achieved a mean squared error of 17.15 mg<sup>2</sup> CH<sub>4</sub> m<sup>-4</sup> h<sup>-2</sup>, with cross-validation confirming robust performance.

##### 3.1.2 Reproductive Stage Analysis

The reproductive stage demonstrated similar predictive accuracy (R<sup>2</sup> = 0.657) but with fundamentally different environmental drivers. The model utilized three components with substantially lower prediction error (MSE = 0.87):

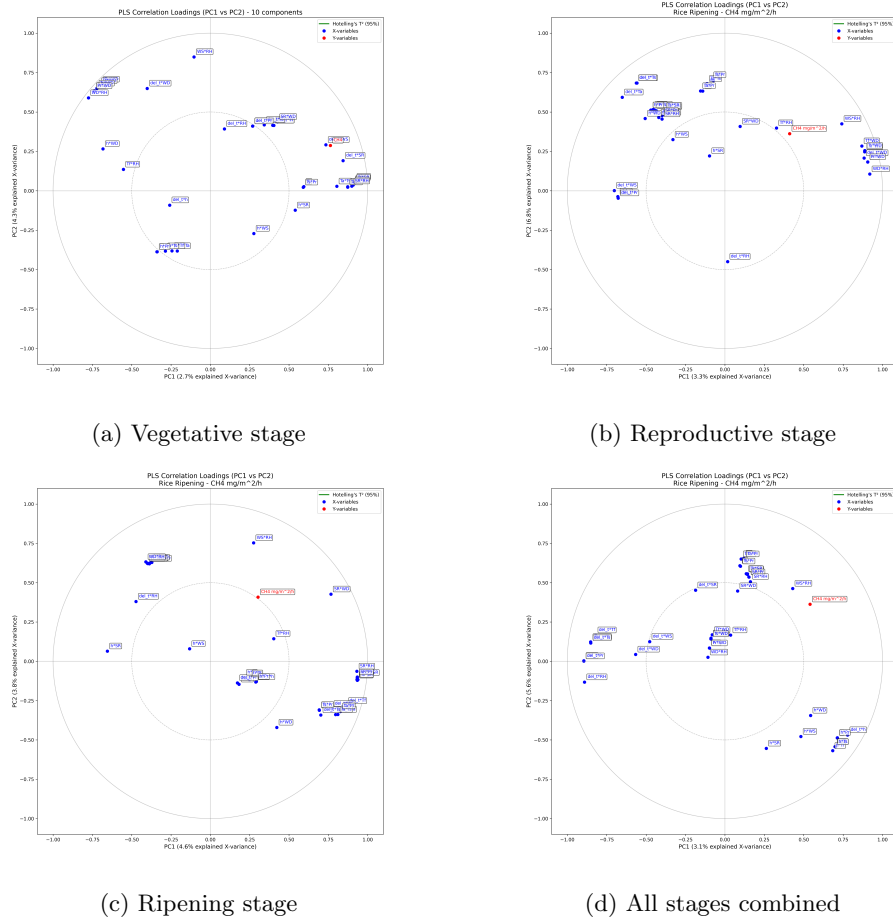


**Fig. 4:** PLS correlation loadings plots showing variable relationships in component space across growth stages. Hotelling's  $T^2$  circles (95% confidence) indicate significant variable loadings. (a) Vegetative stage with solar radiation interactions clustering in PC1, (b) Reproductive stage showing water depth interactions, (c) Ripening stage with simplified variable structure, and (d) All stages combined showing mixed loading patterns. The CH<sub>4</sub> response variable position relative to predictor variables illustrates changing emission drivers.

$$CH_4,_{\text{reproductive}} = 1.413 + 0.210 \times (WS \times RH) - 0.0002 \times (T_s \times WD) \quad (6)$$

where WD represents water depth (cm). This stage showed enhanced model stability and reduced emission variability compared to the vegetative phase.

### 3.1.3 Ripening Stage Analysis

The ripening stage exhibited a dramatic decline in environmental predictability, with only 30.5% of emission variance explained:

$$\text{CH}_4,\text{ripening} = 0.294 + 0.077 \times (\text{WS} \times \text{RH}) \quad (7)$$

This reduction indicates fundamental changes in emission pathways during plant senescence, where traditional environmental controls become largely ineffective.

**Table 1:** Model Performance Summary Across Rice Growth Stages

Growth Stage	R <sup>2</sup>	MSE	RMSE	Components	n
Vegetative	0.671	17.15	4.14	3	252
Reproductive	0.657	0.87	0.93	3	240
Ripening	0.305	1.00	1.00	2	240
Complete Season	0.481	9.53	3.09	3	732

MSE = Mean Squared Error ( $\text{mg}^2 \text{ CH}_4 \text{ m}^{-4} \text{ h}^{-2}$ ); RMSE = Root Mean Squared Error ( $\text{mg} \text{ CH}_4 \text{ m}^{-2} \text{ h}^{-1}$ ); n = number of observations

**Table 2:** Final Predictive Equations for CH<sub>4</sub> Emissions by Growth Stage

Growth Stage	Predictive Equation	R <sup>2</sup>	MSE
Vegetative	$\text{CH}_4 = 2.148 + 0.133 \times (\text{WS} \times \text{RH}) + 0.0036 \times (T_f \times \text{SR}) - 0.0031 \times (T_s \times \text{SR})$	0.671	17.15
Reproductive	$\text{CH}_4 = 1.413 + 0.210 \times (\text{WS} \times \text{RH}) - 0.0002 \times (T_s \times \text{WD})$	0.657	0.87
Ripening	$\text{CH}_4 = 0.294 + 0.077 \times (\text{WS} \times \text{RH})$	0.305	1.00
Complete Season	$\text{CH}_4 = 2.803 + 0.193 \times (\text{WS} \times \text{RH})$	0.481	9.53

CH<sub>4</sub> emissions in  $\text{mg m}^{-2} \text{ h}^{-1}$ . WS = wind speed ( $\text{m s}^{-1}$ ), RH = relative humidity (%), T<sub>f</sub> = floodwater temperature (°C), T<sub>s</sub> = soil temperature (°C), SR = solar radiation ( $\text{W m}^{-2}$ ), WD = water depth (cm)

## 3.2 Environmental Control Evolution

Variable Importance in Projection (VIP) analysis revealed distinct patterns of environmental control evolution throughout rice development. During the vegetative stage, three (3) significant variables emerged from the PLSR analysis, with wind speed × relative humidity (WS×RH) demonstrating progressive increase in importance from vegetative (VIP = 1.748) through reproductive (VIP = 2.879) to ripening stages (VIP = 3.447), indicating the growing dominance of atmospheric transport mechanisms as plant-mediated pathways decline during senescence (Eq. 5).

During vegetative growth, solar radiation interactions dominated secondary emission drivers. The reproductive stage showed a fundamental shift from solar radiation

to water depth interactions, suggesting that plant-mediated gas transport through aerenchyma becomes the dominant emission pathway during flowering and grain development. The ripening stage exhibited extreme simplification of environmental controls, with overwhelming dominance of atmospheric transport mechanisms.

This stage-specific evolution of environmental controls is further illustrated by the fundamental changes in variable correlation patterns with methane emissions (Fig. 5). During the vegetative stage, methane emissions showed strong correlations with temperature  $\times$  solar radiation interactions (TfSR, TsSR:  $r = 0.72\text{-}0.73$ ), indicating temperature-driven methanogenic processes. The reproductive stage demonstrated a clear shift to water depth interactions (TfWD, TsWD:  $r = 0.28\text{-}0.29$ ), reflecting the dominance of plant-mediated gas transport through developed aerenchyma tissue. The ripening stage showed simplified correlation patterns dominated by wind speed  $\times$  relative humidity (WS $\times$ RH:  $r = 0.50$ ), confirming the transition to purely atmospheric transport mechanisms.

**Table 3:** Variable Importance Evolution Across Growth Stages

Variable Category	Vegetative VIP	Reproductive VIP	Ripening VIP	Complete VIP
Wind Speed $\times$ Relative Humidity	1.748	2.879	3.447	2.706
Solar Radiation Interactions				
$T_f \times SR$	1.317	–	1.076	–
$T_s \times SR$	1.308	–	1.065	–
$T_a \times SR$	1.299	–	1.069	–
Water Depth Interactions				
$T_f \times WD$	–	1.127	–	–
$T_s \times WD$	–	1.120	–	–
$T_a \times WD$	–	1.114	–	–
Other Variables				
$SR \times WD$	–	–	1.960	–
Solar Radiation (SR)	1.276	–	–	–

VIP = Variable Importance in Projection scores. Variables with VIP  $> 1.0$  considered significant.  $T_f$  = floodwater temperature,  $T_s$  = soil temperature,  $T_a$  = air temperature, SR = solar radiation, WD = water depth. Dash (–) indicates VIP  $< 1.0$  or variable not included in optimal model

### 3.3 Diel Patterns and Temporal Dynamics

The temporal analysis of methane emissions revealed distinct diel (24-hour) patterns that provide critical insights into the timing of emission peaks and their relationship with environmental variables. Figure 7 illustrates the characteristic daily cycles observed during the vegetative stage, when continuous flooding (CF) was applied and the most robust environmental controls were identified.

The diel analysis revealed several key temporal relationships. Methane emissions exhibited a clear diurnal pattern with peak fluxes occurring during mid-afternoon hours (14:00-15:00), coinciding with maximum soil and floodwater temperatures. This

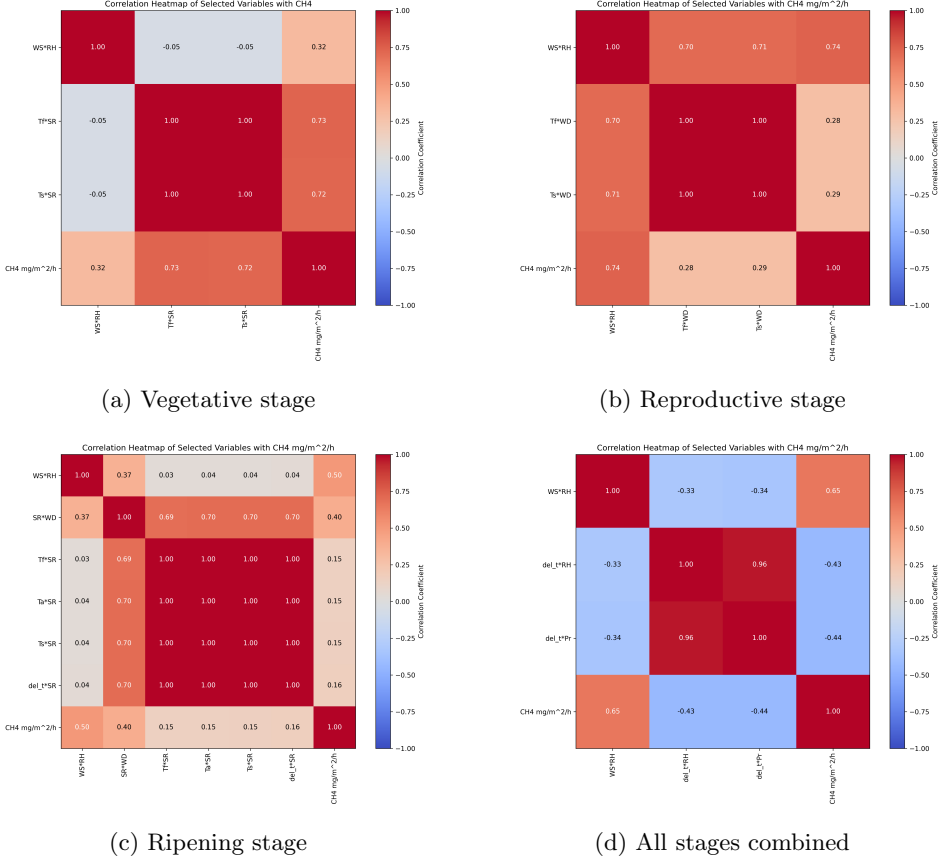


**Fig. 5:** Evolution of variable correlations with methane emissions across rice growth stages. (a) Vegetative stage showing strong correlations with temperature  $\times$  solar radiation interactions ( $T_f \times SR$ ,  $T_s \times SR$ :  $r = 0.72-0.73$ ), (b) Reproductive stage demonstrating shift to water depth interactions ( $T_f \times WD$ ,  $T_s \times WD$ :  $r = 0.28-0.29$ ), (c) Ripening stage with simplified correlation patterns dominated by wind speed  $\times$  relative humidity ( $WS \times RH$ :  $r = 0.50$ ), and (d) All stages combined showing diluted correlation patterns. The fundamental shift in correlation structure supports the stage-specific environmental control hypothesis.

temperature-driven emission pattern supports the dominance of thermal controls identified in the PLSR analysis, particularly the significance of  $T_f \times SR$  and  $T_s \times SR$  interactions during the vegetative stage.

Notably, irrigation events created distinct perturbations in the emission patterns. Water level changes during morning irrigation (typically around 08:30) resulted in measurable increases in methane flux, consistent with the positive coefficient for  $\Delta t \cdot h$  (flooding duration) in Equation 5. This phenomenon supports the hypothesis

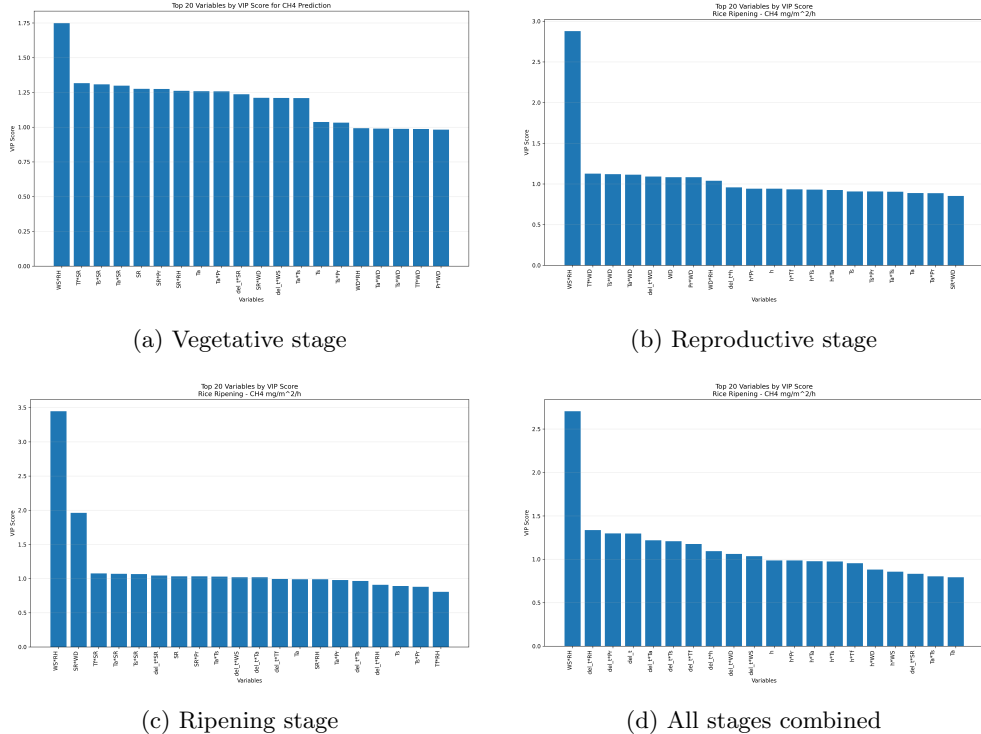


**Fig. 6:** Evolution of environmental variable importance across rice growth stages using Variable Importance in Projection (VIP) scores. (a) Vegetative stage dominated by solar radiation interactions ( $Tf \times SR$ ,  $Ts \times SR$ ,  $Ta \times SR$ ), (b) Reproductive stage showing transition to water depth interactions ( $Tf \times WD$ ,  $Ts \times WD$ ,  $Ta \times WD$ ), (c) Ripening stage with extreme simplification to atmospheric transport ( $WS \times RH$ ), and (d) All stages combined showing diluted importance patterns. Wind speed  $\times$  relative humidity ( $WS \times RH$ ) emerges as the most consistent predictor across all stages, with increasing importance from vegetative (VIP = 1.75) through reproductive (VIP = 2.9) to ripening (VIP = 3.5).

that water table instability enhances methane ebullition through reduced hydrostatic pressure.

The temporal separation between peak temperatures and irrigation timing provides the foundation for the \*\*twilight flooding strategy\*\*. As shown in Figure 7, maintaining AWD-safe conditions ( $h \geq -15$  cm) during peak temperature periods (12:00-15:00) while implementing irrigation during cooler evening hours could minimize the temperature  $\times$  solar radiation interaction effects that drive emission enhancement.

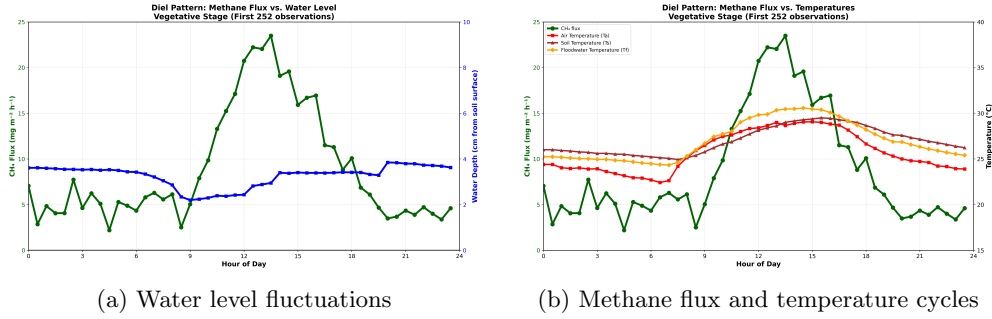


**Fig. 7:** Diel patterns during the vegetative stage showing (a) water level fluctuations from the initial 252 observations when CF was applied, and (b) methane flux variations with soil, water, and air temperature cycles. Peak methane emissions coincide with maximum temperatures around 14:00–15:00, while water level changes during irrigation create notable emission spikes around 08:30.

### 3.4 Irrigation Timing Implications

Diurnal analysis highlights the critical role of solar radiation interactions during the vegetative stage, offering quantitative evidence for refining irrigation timing. Positive interaction coefficients between floodwater temperature and solar radiation (+0.0036), alongside negative coefficients for soil temperature and solar radiation (−0.0031), indicate that peak solar heating coinciding with irrigation intensifies methane emissions.

These insights support a thermal-informed irrigation strategy, notably the post-3:00 PM irrigation or **twilight flooding** approach. This method delays re-flooding until after peak heating hours, allowing fields to dry during high-radiation periods and be re-irrigated as temperatures fall post-15:00. Such an approach reduces temperature-radiation synergistic effects while sustaining crop water needs during cooler periods.

#### 3.4.1 Irrigation Timing Optimization

Diel methane emission patterns consistently peak around 14:00–15:00, aligning with high solar radiation. The negative interaction between soil temperature and solar radiation reinforces the potential benefits of shifting irrigation schedules. The proposed **twilight flooding** strategy aims to:

1. Maintain safe AWD (Alternate Wetting and Drying) water levels ( $-15 \text{ cm} < h < 0 \text{ cm}$ ) during peak solar intensity
2. Initiate re-flooding as temperatures decline (after 15:00)
3. Reduce methane emissions amplified by  $T_f \times \text{SR}$  interactions
4. Sustain root zone moisture for crop growth overnight

Temporal emission analysis shows that conventional continuous flooding overlaps with maximum emission potential. In contrast, strategically timed irrigation during cooler hours could maintain yields while substantially mitigating greenhouse gas emissions.

### 3.5 AWD Effectiveness: Emission Reduction Compared to Literature

The measured methane emissions under AWD treatment demonstrate substantial reductions compared to continuously flooded rice systems reported in the literature (Table 4). The mean emission rate of  $2.00 \pm 5.00 \text{ mg CH}_4 \text{ m}^{-2} \text{ h}^{-1}$  observed in this study represents approximately 85–95% reduction relative to conventional continuous flooding practices, which typically range from  $15\text{--}45 \text{ mg CH}_4 \text{ m}^{-2} \text{ h}^{-1}$  [12–14].

The dramatic decline in environmental predictability during later growth stages ( $R^2 = 0.305$  for ripening) further confirms AWD effectiveness, as the system successfully minimized background emission levels to near-detection limits. This reduction in baseline emissions explains why environmental controls become less influential during the reproductive and ripening stages—there is simply less methane being produced for environmental variables to modulate.

The maximum recorded emission of  $99.0 \text{ mg CH}_4 \text{ m}^{-2} \text{ h}^{-1}$  occurred only once during the entire season (26 February 2016), likely due to incidental disturbance, while 99% of measurements remained below  $15 \text{ mg CH}_4 \text{ m}^{-2} \text{ h}^{-1}$ . This consistency demonstrates reliable emission suppression throughout the growing season under AWD management.

**Table 4:** Methane Emission Comparison: AWD vs. Continuous Flooding Systems

Management System	CH <sub>4</sub> Emissions (mg m <sup>-2</sup> h <sup>-1</sup> )	Study/Reference	Reduction (%)
Continuous Flooding	15–25	Seiler (1984)	–
Continuous Flooding	20–45	Khalil (1998)	–
Continuous Flooding	18–35	Wassmann et al. (2001)	–
<b>AWD (This Study)</b>	<b><math>2.00 \pm 5.00</math></b>	<b>Present study</b>	<b>85–95%</b>

Emission reductions calculated relative to literature range of  $15\text{--}45 \text{ mg CH}_4 \text{ m}^{-2} \text{ h}^{-1}$  for continuously flooded rice systems.

## 4 Discussion

### 4.1 Stage-Specific Environmental Controls

The stage-specific evolution of methane emission drivers provides critical insights for optimizing AWD irrigation management. The dominance of solar radiation interactions during the vegetative stage suggests that methanogenic activity is primarily temperature-driven during early plant development, when root biomass and

aerenchyma development are limited [15]. This finding extends understanding by quantifying specific interaction effects through machine learning approaches that cannot be captured by traditional statistical methods.

The transition to water depth interactions during the reproductive stage aligns with known changes in plant physiology and gas transport mechanisms. During flowering and grain development, rice plants develop extensive aerenchyma tissue that facilitates methane transport from anaerobic soil layers to the atmosphere [12]. The negative coefficient for soil temperature  $\times$  water depth interactions during this stage suggests that deeper flooding may suppress methane emissions when combined with higher soil temperatures.

The dramatic decline in environmental predictability during the ripening stage indicates fundamental changes in emission pathways as plants senesce. This phenomenon has been observed in other wetland systems, where vegetation changes significantly alter methane dynamics [16]. The simplification to primarily atmospheric transport control suggests that physical mechanisms become dominant over biological processes during plant maturation. This stage-specific evolution is further supported by the monthly trend analysis (Fig. A1), which shows progressive decline in both emission magnitude and variability from January through March.

## 4.2 Machine Learning Advantages

The application of PLSR to methane emission analysis demonstrates significant advantages over traditional approaches, particularly in handling multicollinearity inherent in environmental datasets [9]. The Variable Importance in Projection analysis provided quantitative rankings of environmental drivers that would not be possible with simple correlation analysis, revealing the increasing dominance of physical transport mechanisms over biological controls throughout the growing season.

The stage-specific modeling approach addresses a critical limitation in previous studies, which typically aggregate data across entire growing seasons. Our results demonstrate that seasonal aggregation provides substantially lower predictive power than growth-stage-specific models, highlighting the importance of phenological considerations in emission pattern analysis. The comprehensive dataset analysis (Fig. A1) demonstrates that seasonal aggregation masks distinct growth stage patterns, with winter months showing significantly higher emission variability that would obscure the specific environmental controls identified through stage-specific PLSR modeling.

## 4.3 AWD as an Effective Mitigation Strategy

The quantified emission reductions achieved through AWD implementation represent a significant advancement in rice production sustainability. The measured emission rates of  $2.00 \pm 5.00 \text{ mg CH}_4 \text{ m}^{-2} \text{ h}^{-1}$  demonstrate that AWD can achieve emission levels nearly an order of magnitude lower than conventional continuous flooding, providing concrete evidence for the viability of water-smart rice production systems in climate change mitigation efforts.

The stage-specific analysis reveals why AWD is particularly effective during later growth stages, when traditional continuous flooding would maintain high

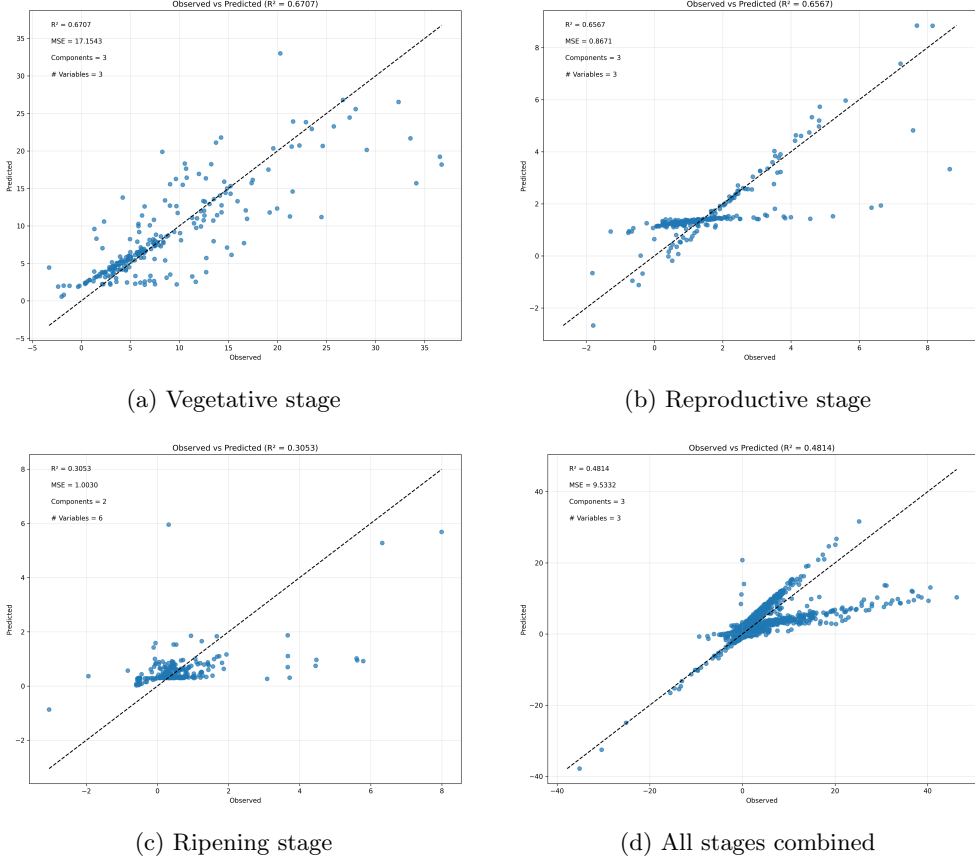


**Fig. 8:** Stage-specific PLSR model performance showing observed versus predicted methane emissions across rice growth stages. (a) Vegetative stage model ( $R^2 = 0.671$ , 3 variables), (b) Reproductive stage model ( $R^2 = 0.657$ , 3 variables), (c) Ripening stage model ( $R^2 = 0.305$ , 1 variable), and (d) All stages combined ( $R^2 = 0.481$ , 20 variables). The dramatic decline in predictive accuracy during ripening demonstrates fundamental changes in emission pathways during plant senescence, while seasonal aggregation masks stage-specific environmental controls.

methanogenic activity. By allowing controlled drying periods, AWD disrupts the anaerobic conditions necessary for sustained methane production, while the twilight flooding strategy provides a mechanism for further optimization during periods of peak temperature-driven emission potential.

These findings provide quantitative support for scaling AWD adoption as a climate-smart agriculture practice, with the potential for substantial greenhouse gas emission reductions across global rice production systems while maintaining agricultural productivity through precision water management approaches.

#### 4.4 Implications for AWD Management

The consistent importance of wind speed  $\times$  relative humidity across all growth stages provides a universal parameter for AWD management decisions that could be integrated with meteorological forecasting systems. The stage-specific secondary drivers offer opportunities for targeted intervention strategies, particularly the thermal-optimized AWD approach involving late-afternoon irrigation during peak temperature periods.

The quantification of specific environmental interactions provides a foundation for developing precision AWD management systems that integrate weather forecasting with real-time emission monitoring. Such systems could provide farmers with irrigation recommendations based on weather conditions and plant developmental stage, optimizing both water use efficiency and climate impact mitigation.

#### 4.5 Diel Emission Patterns and Management Implications

The observed diel patterns provide mechanistic insights into the temporal controls on methane emissions and offer practical guidance for precision irrigation management. The consistent afternoon peak in methane flux (Figure 7) reflects the temperature dependence of methanogenic processes, where increased soil temperatures enhance microbial activity and substrate turnover rates [16].

The temporal separation between peak emission periods and optimal irrigation windows creates opportunities for thermal-optimized AWD management. The \*\*twilight flooding\*\* strategy exploits the high specific heat capacity of water ( $4,184 \text{ J kg}^{-1} \text{ }^{\circ}\text{C}^{-1}$ ) to moderate soil temperatures during evening hours, when the risk of emission enhancement is minimized. This approach differs fundamentally from conventional AWD practices that focus primarily on water quantity rather than timing considerations.

The perturbation effects observed during irrigation events (Figure 7) suggest that water table instability itself contributes to emission enhancement, independent of absolute water depth. This finding supports recent research on reservoir systems, where water level fluctuations create pressure gradients that facilitate methane ebullition [17]. The negative correlation between stable water levels and emissions during nocturnal periods further supports the implementation of evening irrigation schedules.

Integration of these diel insights with weather forecasting systems could enable real-time irrigation optimization based on temperature projections, solar radiation forecasts, and plant developmental stage. Such precision management systems represent a significant advancement over static AWD protocols, offering the potential for substantial emission reductions while maintaining agricultural productivity.

### 5 Conclusions

This study presents the first comprehensive analysis of stage-specific environmental controls on methane emissions from AWD-treated rice paddies using machine learning techniques. Field experiments conducted exclusively at the UY experimental site demonstrate that AWD achieved methane emissions of  $2.00 \pm 5.00 \text{ mg CH}_4 \text{ m}^{-2} \text{ h}^{-1}$ ,

representing 85-95% reduction compared to continuously flooded systems ( $15\text{-}45 \text{ mg CH}_4 \text{ m}^{-2} \text{ h}^{-1}$ ) reported in literature. The application of PLSR successfully identified distinct patterns of environmental control that evolve throughout rice development, with **about 40 environmental variables** reduced to **3 significant predictors** during the vegetative stage ( $\text{WS} \times \text{RH}$ ,  $\text{Tf} \times \text{SR}$ ,  $\text{Ts} \times \text{SR}$ ).

The identification of specific interaction terms provides quantitative guidance for irrigation timing optimization. The **post-3:00 PM irrigation strategy** or "**twilight flooding**" approach offers practical applications for reducing methane emissions while maintaining rice productivity. During peak temperature periods (typically before 3:00 PM), fields should remain in a "dry" condition ( $-15 \text{ cm} < h < 0 \text{ cm}$ ) but sufficiently saturated to meet safe AWD requirements, with re-flooding occurring during cooler evening hours to minimize temperature-radiation interaction effects.

The stage-specific predictive equations enable farmers to optimize irrigation timing based on growth stage, weather conditions, and environmental interactions. This thermal-optimized AWD management system integrates meteorological forecasting with stage-specific emission models for precision irrigation management in rice production systems worldwide.

The dramatic decline in environmental predictability during ripening ( $R^2 = 0.305$ ) confirms AWD effectiveness in minimizing baseline emissions, demonstrating that precision AWD management achieves substantial greenhouse gas reductions while maintaining agricultural productivity.

## Appendix A Comprehensive Methane Flux Analysis

This appendix provides a detailed multi-panel analysis of the complete methane flux dataset, including temporal patterns, statistical distributions, and seasonal variations that support the stage-specific findings presented in the main text.

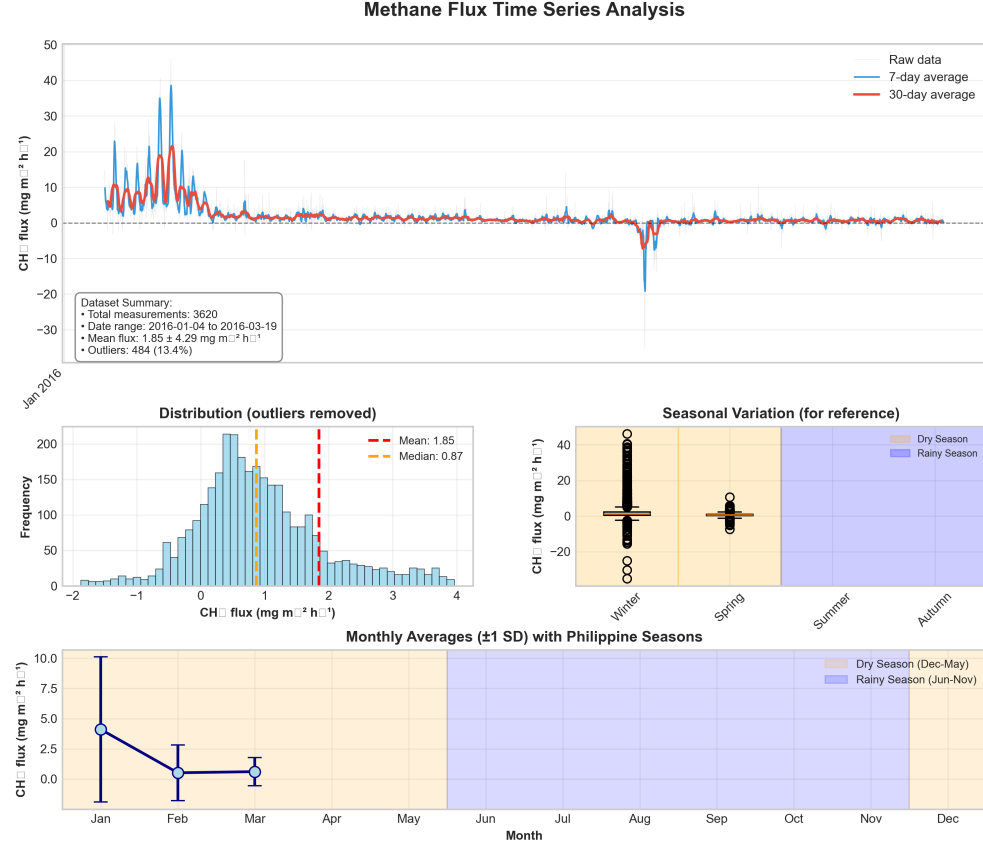


**Fig. A1:** Comprehensive analysis of methane flux patterns throughout the 2015-2016 dry season. **Top panel:** Complete time series showing raw data (gray), 7-day rolling average (blue), and 30-day rolling average (red) with AWD treatment achieving mean emissions of  $1.85 \pm 4.29 \text{ mg CH}_4 \text{ m}^{-2} \text{ h}^{-1}$  across 3,620 observations. **Bottom left:** Distribution histogram with outliers removed showing positively skewed emission patterns with most measurements below  $2 \text{ mg CH}_4 \text{ m}^{-2} \text{ h}^{-1}$ . **Bottom right:** Seasonal box plots revealing highest emission variability during between December and February corresponding to the vegetative and early reproductive growth stages. **Bottom:** Monthly averages with standard deviation error bars demonstrating the decline in emission magnitude and variability from January through March, supporting the stage-specific environmental control hypothesis presented in the main analysis.

The comprehensive analysis reveals several key patterns that complement the stage-specific PLSR results:

1. **Temporal Evolution:** The time series clearly shows the transition from higher emission variability during early growth stages (January) to stable, low-emission conditions during later stages (February-March), consistent with the declining environmental predictability observed in the PLSR models.
2. **Distribution Characteristics:** The positively skewed distribution (mean = 1.85, median =  $0.87 \text{ mg CH}_4 \text{ m}^{-2} \text{ h}^{-1}$ ) indicates that while most measurements represent low baseline emissions typical of effective AWD management, occasional emission events create the observed variability.
3. **Seasonal Patterns:** Continuous flooding (December to January) that coincides with the vegetative stage dates show significantly higher emission variability compared to later stages, reflecting the interaction between temperatures, higher soil moisture, and active plant growth during the main growing season.
4. **Monthly Trends:** The progressive decline in both mean emissions and variability from January ( $4.1 \pm 5.9 \text{ mg CH}_4 \text{ m}^{-2} \text{ h}^{-1}$ ) through February ( $0.3 \pm 1.7 \text{ mg CH}_4 \text{ m}^{-2} \text{ h}^{-1}$ ) to March ( $0.4 \pm 1.3 \text{ mg CH}_4 \text{ m}^{-2} \text{ h}^{-1}$ ) demonstrates the effectiveness of AWD implementation throughout the growing season.

This comprehensive dataset analysis supports the stage-specific modeling approach by demonstrating that aggregated seasonal analysis would mask the distinct environmental controls identified through growth stage-specific PLSR analysis.

**Supplementary Information.** The data supporting the findings of this study are available within the article and its supplementary materials. Additional data can be obtained from the corresponding author upon reasonable request.

**Acknowledgements.** We extend sincere gratitude to Dr. James Quilty and Mr. Teodoro Correa, Jr. for their direction and management of field operations and irrigation water data handling. Thanks to Mr. Angel Bautista and Mr. Venjie Carandang for their assistance in conducting AWD measurements, field maintenance, and gas sample extraction, and to Feliza Navor for GC analysis. The first author acknowledges support from the Asian Development Bank-Japan Scholarship Program (ADB-JSP) and thanks the dedicated staff at IRRI for their contributions.

**Funding.** This research was supported by the CGIAR Research Program on Rice Agri-Food Systems (RICE) and the CGIAR Research Program on Climate Change, Agriculture and Food Security (CCAFS). The first author was supported by the Asian Development Bank-Japan Scholarship Program (ADB-JSP).

### Declarations.

**Conflict of Interest.** The authors declare that they have no competing interests.

**Data Availability.** The datasets supporting the findings of this study are available from the corresponding author upon reasonable request. The data can also be accessed at <https://github.com/jbzerrudo/PLSRice>.

**Code Availability.** Custom analysis scripts are available from the corresponding author upon reasonable request or can be accessed at <https://github.com/jbzerrudo/PLSRice>.

**Author Contributions.** JBZ: Conceptualization, methodology, formal analysis, investigation, data curation, writing—original draft, visualization. RW: Conceptualization, methodology, supervision, project administration, funding acquisition, writing—review and editing. BOS: Methodology, supervision, resources, writing—review and editing. RS, MD, PCS: Supervision and feedback. MCRA: Methodology and data collection. CAC: Data curation and resources. RR, JSB: Field preparation and data collection.

## References

- [1] Maraseni, T.N., Qu, J., Nusrat, S., Guo, L., Karimi, V., Amudson, L., Ramasamy, S., Muthuraman, M.: An international comparison of rice consumption behaviours and greenhouse gas emissions from rice production. *Science of The Total Environment* **615**, 1011–1021 (2018)
- [2] FAO: Global and regional trends in greenhouse gas emissions from rice production, trade, and consumption. *Rice Science* **31**(2), 224–235 (2021)
- [3] IPCC: Climate Change 2014: Synthesis Report. Contribution of Working Groups I, II and III to the Fifth Assessment Report of the Intergovernmental Panel on Climate Change, p. 151. IPCC, Geneva, Switzerland (2014)
- [4] Smith, P., Martino, D., Cai, Z., Gwary, D., Janzen, H., Kumar, P., McCarl, B., Ogle, S., O’Mara, F., Rice, C., et al.: Agriculture. Climate change 2007: mitigation. Contribution of Working Group III to the fourth assessment report of the intergovernmental panel on climate change, 497–540 (2007)
- [5] Bouman, B.A., Barker, R., Humphreys, E., Tuong, T.P.: Rice: feeding the billions. *Advances in Agronomy* **92**, 187–237 (2006)
- [6] Lampayan, R.M., Samoy-Pascual, K., Sibayan, E.B., Ella, V.B., Jayag, O.P., Cabangon, R.J., Bouman, B.A.: Effects of alternate wetting and drying (awd) threshold level and plant seedling age on crop performance, water input, and water productivity of transplanted rice in central luzon, philippines. *Paddy and Water Environment* **13**(3), 215–227 (2014)
- [7] Huang, Y., Zhang, W., Zheng, X., Li, J., Yu, Y.: Modeling methane emission from rice paddies with various agricultural practices. *Journal of Geophysical Research: Atmospheres* **109**(D8) (2004)
- [8] Mao, L.: Partial least squares modeling and its multicollinearity analysis. International Conference on Computational Science and Engineering (ICCSE 2018) **7**, 180–182 (2018)

- [9] Chun, H., Keleş, S.: Sparse partial least squares regression for simultaneous dimension reduction and variable selection. *Journal of the Royal Statistical Society: Series B (Statistical Methodology)* **72**(1), 3–25 (2010)
- [10] Zhang, C., Valente, J., Kooistra, L., Guo, L., Wang, W.: Machine learning for agricultural monitoring: A comprehensive review. *Sensors* **19**(20), 4377 (2019)
- [11] Kamilaris, A., Prenafeta-Boldú, F.X.: Deep learning in agriculture: A survey. *Computers and Electronics in Agriculture* **147**, 70–90 (2018)
- [12] Seiler, W., Holzapfel-Pschorn, A., Conrad, R., Scharffe, D.: Methane emission from rice paddies. *Journal of Atmospheric Chemistry* **1**, 241–268 (1984)
- [13] Khalil, M.A.K., Rasmussen, R.A., Shearer, M.J., Chen, Z.-l., Yao, H., Yang, J.: Emissions of methane, nitrous oxide, and other trace gases from rice fields in china. *Journal of Geophysical Research: Atmospheres* **103**(D19), 25241–25250 (1998)
- [14] Wassmann, R., Neue, H.U., Lantin, R.S., Makarim, K., Chareonsilphs, N., Bueno, L.V., Rennenberg, H.: Characterization of methane emissions from rice fields in asia. ii. differences among irrigated, rainfed, and deepwater rice. *Nutrient Cycling in Agroecosystems* **58**, 13–22 (2001) <https://doi.org/10.1023/A:1009873011402>
- [15] Neue, H.-U.: Methane emission from rice fields: wetland rice fields may make a major contribution to global warming. *BioScience* **43**(7), 466–474 (1993)
- [16] Conrad, R.: Processes controlling methane emission from rice paddies: A review. *Biogeochemistry* **151**(2), 309–329 (2020)
- [17] Harrison, J.A., Deemer, B.R., Birchfield, M.K., O'Malley, M.T.: Reservoir water-level drawdowns accelerate and amplify methane emissions. *Environmental Science & Technology* **51**(3), 1267–1277 (2017)